Molecular Cell, Vol. 15, 999–1006, September 24, 2004, Copyright ©2004 by Cell Press

Structural, Biochemical, and Functional Analyses of CED-9 Recognition by the Proapoptotic Proteins EGL-1 and CED-4

Nieng Yan,[1,4] Lichuan Gu,[1,4] David Kokel,[2,4] Jijie Chai,[1] Wenyu Li,[1] Aidong Han,[3] Lin Chen,[3] Ding Xue,[2] and Yigong Shi[1,*]
[1]Department of Molecular Biology
Princeton University
Lewis Thomas Laboratory
Washington Road
Princeton, New Jersey 08544
[2]Department of Molecular, Cellular and Developmental Biology
[3]Department of Chemistry and Biochemistry
University of Colorado
Boulder, Colorado 80309

Summary

Programmed cell death in *Caenorhabditis elegans* is initiated by the binding of EGL-1 to CED-9, which disrupts the CED-4/CED-9 complex and allows CED-4 to activate the cell-killing caspase CED-3. Here we demonstrate that the C-terminal half of EGL-1 is necessary and sufficient for binding to CED-9 and for killing cells. Structure of the EGL-1/CED-9 complex revealed that EGL-1 adopts an extended α-helical conformation and induces substantial structural rearrangements in CED-9 upon binding. EGL-1 interface mutants failed to bind to CED-9 or to release CED-4 from the CED-4/CED-9 complex, and were unable to induce cell death in vivo. A surface patch on CED-9, different from that required for binding to EGL-1, was identified to be responsible for binding to CED-4. These data suggest a working mechanism for the release of CED-4 from the CED-4/CED-9 complex upon EGL-1 binding and provide a mechanistic framework for understanding apoptosis activation in *C. elegans*.

Introduction

Genetic analysis of programmed cell death in *Caenorhabditis elegans* has identified four genes, *egl-1*, *ced-9*, *ced-4*, and *ced-3*, that control the death of 131 somatic cells during hermaphrodite development (Horvitz, 1999, 2003). CED-3 belongs to the caspase family (Xue et al., 1996; Yuan et al., 1993), which is a cysteine protease and cleaves its substrates after an aspartate residue (Shi, 2002). CED-3 is synthesized as an inactive zymogen. During apoptosis, the CED-3 zymogen is activated by the adaptor molecule CED-4 (Chinnaiyan et al., 1997; Irmler et al., 1997; Seshagiri and Miller, 1997; Wu et al., 1997a; Yang et al., 1998; Yuan and Horvitz, 1992). However, in the absence of an apoptotic stimulus, CED-4 is sequestered by the mitochondria-bound CED-9 (Chen et al., 2000; Chinnaiyan et al., 1997; Hengartner and Horvitz, 1994b; James et al., 1997; Spector et al., 1997; Wu et al., 1997b), unable to activate CED-3. The CED-4/CED-9 interaction is disrupted by the proapoptotic protein EGL-1 (Conradt and Horvitz, 1998; del Peso et al., 1998, 2000), which is transcriptionally activated by upstream apoptotic signals. A 5 bp deletion in *egl-1* (*n3082*), which leads to the production of only the N-terminal 45 amino acids of the wild-type (WT) EGL-1 protein, blocked almost all somatic cell deaths (Conradt and Horvitz, 1998).

The binding of EGL-1 to CED-9 is central to the initiation of apoptosis. CED-9 shares significant sequence homology with the mammalian antiapoptotic proteins, Bcl-2 and Bcl-xL (Hengartner and Horvitz, 1994b), whereas EGL-1 resembles the proapoptotic BH3-only proteins (such as Bad and Bim [Cory et al., 2003; Puthalakath and Strasser, 2002]) and contains a conserved 9 residue BH3 motif (Conradt and Horvitz, 1998). Interestingly, a previous structural study on the isolated CED-9 protein did not reveal the presence of a BH3 binding surface groove on CED-9 and predicted a novel mode of interaction (Woo et al., 2003).

Results and Discussion

Characterization of EGL-1/CED-9 Interactions

To determine the mechanism of CED-9 recognition by EGL-1, we characterized the EGL-1/CED-9 interaction (Figure 1A). Various fragments of the GST-EGL-1 protein were evaluated for their ability to interact with the CED-9 protein (residues 1–251). The N-terminal half (residues 1–45) of EGL-1 did not show detectable binding to CED-9. In contrast, the C-terminal half (residues 45–87 or 45–91) formed a stable complex with CED-9 (Figure 1A). Using a similar strategy, residues 68–237 of CED-9 were found to be the minimal structural core that is necessary and sufficient for binding to EGL-1 (data not shown). Removal of four hydrophobic residues ($F_{88}F_{89}A_{90}F_{91}$) at the C terminus of EGL-1 did not affect its binding to CED-9 (Figure 1A) but significantly improved expression levels of the recombinant proteins.

To identify EGL-1 residues that are important for CED-9 binding, we introduced a number of missense mutations into EGL-1 and assessed the ability of the resulting EGL-1 variants to interact with CED-9. Mutation of two residues in EGL-1, G55E and F65A, completely abolished its interaction with CED-9 (Figure 1A), suggesting a critical role by these two residues in mediating EGL-1/CED-9 interaction.

Structure of an EGL-1/CED-9 Complex

To reveal the mechanism of CED-9 recognition by EGL-1, we crystallized CED-9 (residues 68–237) in complex with EGL-1 (residues 45–87 or 31–87). The crystallization process proved to be treacherous, and the needle-shaped crystals were obtained after extensive effort involving more than 100 different EGL-1/CED-9 complexes over 30,000 crystallization conditions. The structure was determined by molecular replacement and refined to 2.2 Å resolution (Table 1; Figure 1B).

The EGL-1/CED-9 complex adopts a compact, globu-

*Correspondence: yshi@molbio.princeton.edu
[4]These authors contributed equally to this work.

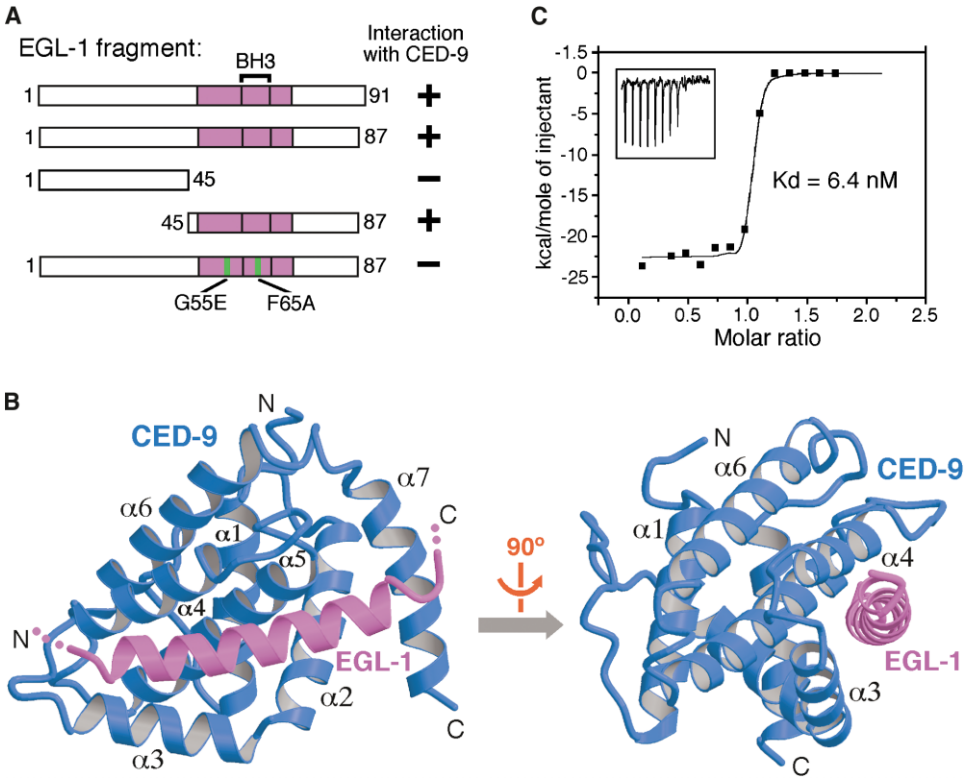

Figure 1. Biochemical and Structural Analysis of the EGL-1/CED-9 Complex

(A) Summary of binding studies between CED-9 (residues 1–251) and various EGL-1 fragments. The C-terminal half of EGL-1 (residues 45–87) was found to be necessary and sufficient for binding to CED-9.

(B) Overall structure of an EGL-1/CED-9 complex. CED-9 and EGL-1 are colored cyan and pink, respectively. Only 27 amino acids of EGL-1 (47–73) contribute to CED-9 binding and are visible in the electron density map.

(C) Measurement of binding affinities between EGL-1 and CED-9 by isothermal titration calorimetry (ITC). Shown here is a representative ITC run between CED-9 (residues 68–251) and EGL-1 (48–72). Data fitting revealed a binding affinity of 6.4 nM, similar to that between CED-9 and the full-length EGL-1.

lar fold, resembling a single folding unit (Figure 1B). CED-9 comprises seven α helices, with the central hydrophobic helix α5 surrounded by six helices and several surface loops. A 27 amino acid fragment of the EGL-1 protein (residues 47–73) forms a single amphipathic α helix, packing against CED-9 helices α2, α3, α4, α5, and α7 over an extended hydrophobic surface cleft (Figure 1B). Residues N- or C-terminal to the EGL-1 helix were disordered in the crystals and thus are not involved in binding to CED-9. To confirm that these regions of EGL-1 do not contribute to CED-9 binding, we examined the binding affinities between CED-9 and various fragments of EGL-1 using isothermal titration calorimetry (ITC). The results revealed that the EGL-1 fragment (residues 48–72) binds to CED-9 (residues 68–251) with a dissociation constant of 6.4 nM (Figure 1C), nearly identical to that of the full-length EGL-1 protein to CED-9 (6.7 nM; data not shown).

Compared to the free CED-9 protein, EGL-1-bound CED-9 undergoes significant structural rearrangements, leading to the exposure of an extended hydrophobic surface cleft (Figure 2A). Nonpolar residues from the amphipathic EGL-1 helix interact with this hydrophobic surface cleft on CED-9. This interaction results in the burial of 2454 Å^2 exposed surface area. To configure this surface cleft, residues on helix α4 of CED-9 are translocated over a distance of 8–12 Å (Figure 2B). This unusual conformational flexibility might underlie the critical functions of CED-9 and other Bcl-2 family proteins.

The conformational change observed in the EGL-1/CED-9 complex is quite different from that reported in the mammalian complexes involving Bcl-xL. In those cases, the change primarily involves a lateral movement of helix α3, such as that in the Bak-BH3/Bcl-xL complex (Sattler et al., 1997). However, in the EGL-1/CED-9 complex, helix α3 remains nearly unchanged before and after EGL-1 binding, yet helix α4 undergoes drastic structural rearrangements (Figure 2B). In addition, the EGL-1/CED-9 interface is more extensive than that of the reported mammalian complexes involving Bcl-xL and a BH3 peptide (Liu et al., 2003; Petros et al., 2000; Sattler et al., 1997), as judged by the number of van der Waals contacts and the extent of buried surface area.

The EGL-1/CED-9 Interface

The driving force for the binding of EGL-1 to CED-9 is van der Waals interactions. Nine hydrophobic side chains as well as two glycine residues (Gly51 and Gly55) from the amphipathic EGL-1 helix make extensive contacts to the hydrophobic surface cleft on CED-9 (Figure 3A). At

Table 1. Data Collection and Statistics from Crystallographic Analysis

Beam line	CHESS-A1
Space group	$P4_3$
Resolution (Å)	99.0–2.2 Å
Total observations	129,470
Unique observations	25,287
Data coverage (outer shell)	99.8% (99.7%)
R_{sym} (outer shell)	0.083 (0.486)
Refinement	
Resolution range (Å)	20.0–2.2 Å
Number of reflections ($\|F\| > 0$)	24,864
Data coverage (outer shell)	97.5% (88.2%)
$R_{working}/R_{free}$	0.215/0.235
Number of atoms	3,138
Number of waters	116
Rmsd bond length (Å)	0.010
Rmsd bond angles (°)	1.68
Ramachandran Plot	
Most favored (%)	90.6
Additionally allowed (%)	7.9
Generously allowed (%)	1.5
Disallowed (%)	0.0

$R_{sym} = \Sigma_h\Sigma_i|I_{h,i} - I_h|/\Sigma_h\Sigma_i I_{h,i}$, where I_h is the mean intensity of the i observations of symmetry related reflections of h. $R = \Sigma|F_{obs} - F_{calc}|/\Sigma F_{obs}$, where $F_{obs} = F_P$, and F_{calc} is the calculated protein structure factor from the atomic model (R_{free} was calculated with 5% of the reflections). Rmsd in bond lengths and angles are the deviations from ideal values, and the rmsd deviation in B factors is calculated between bonded atoms.

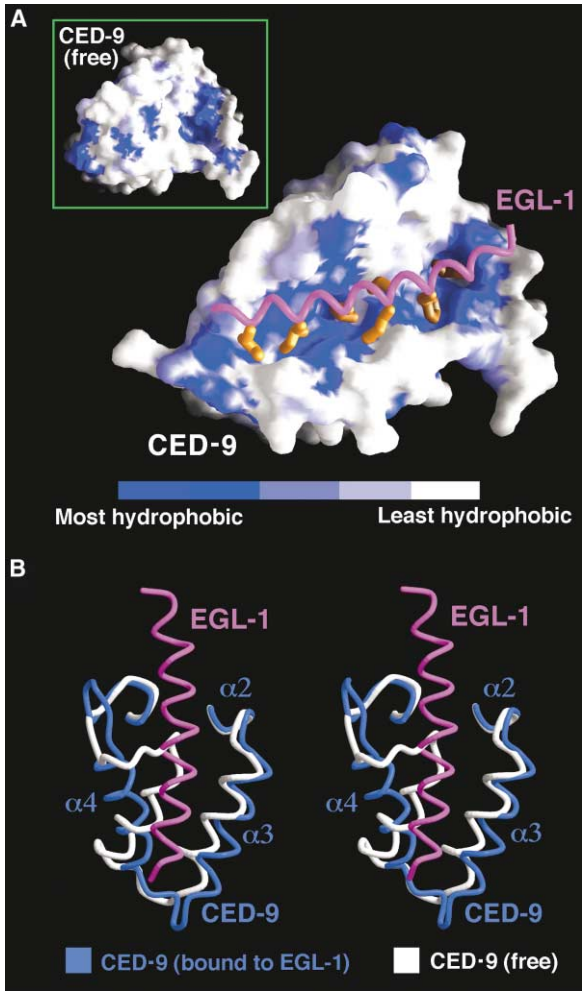

Figure 2. EGL-1 Binding Induces Significant Structural Rearrangements in CED-9

(A) A surface representation of the EGL-1-bound CED-9 and the free CED-9 (inset). These two CED-9 molecules are in the same orientation and can be superimposed with each other with 1.23 Å root-mean-square deviation (rmsd). Note the absence of a hydrophobic surface cleft in the free CED-9.

(B) Structural comparison of the EGL-1-bound CED-9 (cyan) and the free CED-9 (gray). For clarity, only regions of CED-9 surrounding the bound EGL-1 fragment are shown. Helix α4 and the following loop undergo drastic rearrangements upon binding to EGL-1.

the N-terminal portion of the EGL-1 helix, two isoleucines (Ile50 and Ile54) and two glycines (Gly51 and Gly55) stack against the wedge between helices α3 and α4 of CED-9 (Figure 3A). At the center of the interface, Phe65 of EGL-1 is nestled in a hydrophobic pocket formed by CED-9 residues Met119, Phe123, Lys126, Ile 172, and Met231, whereas Met61 of EGL-1 interacts with Phe123, Phe131, Phe134, and His127 of CED-9. At the C-terminal portion of the EGL-1 helix, there are six intermolecular hydrogen bonds in addition to van der Waals contacts between Met69/Met70 of EGL-1 and surrounding CED-9 residues (Figure 3A). In particular, the carboxylate side chains of Asp63 and Asp66 make a pair of charge-stabilized hydrogen bonds to Arg170 and Arg219 of CED-9, respectively (Figure 3A).

The key residues of EGL-1 that interact with CED-9 are highly conserved between *C. elegans* and *C. briggsae*, two related nematodes species (Figure 3B). Interestingly, residues from the predicted BH3 domain (Leu58–Asp66) only contribute to approximately half of the observed interactions and one-third of the extended EGL-1 helix (Figure 3B). This structural finding nicely explains the observation that the EGL-1 BH3 peptide does not stabilize the CED-9 protein to the same extent as the intact EGL-1 protein (Woo et al., 2003).

Biochemical and Functional Analyses of EGL-1/CED-9 Interactions

To corroborate our structural analysis, we examined whether mutations on the interface residues of EGL-1 could weaken or disrupt its binding to CED-9. Various mutant EGL-1 fragments were purified as fusion proteins with glutathione S-transferase (GST), and their interactions with CED-9 were investigated using a GST-mediated pull-down assay (Figure 3C). Consistent with the observed structural features, substitution of a bulky hydrophobic residue (Leu58, Met61, Phe65, or Met69) by Ala in EGL-1 did not significantly affect its interaction with CED-9 (Figure 3C, lanes 8 and 10–13). Strikingly, substitution of Gly55 by a negatively charged glutamate residue was not sufficient to abolish interaction with CED-9 (lane 9). Nonetheless, a double mutant (mut2, G55E/F65A) and a quadruple mutant (mut4, G55E/L58A/F65A/M69A) failed to bind to CED-9 (lanes 4, 6, and 7). These results are consistent with the structural observation that the intimate interface between EGL-1 and CED-9 closely resembles the interior of a single folded

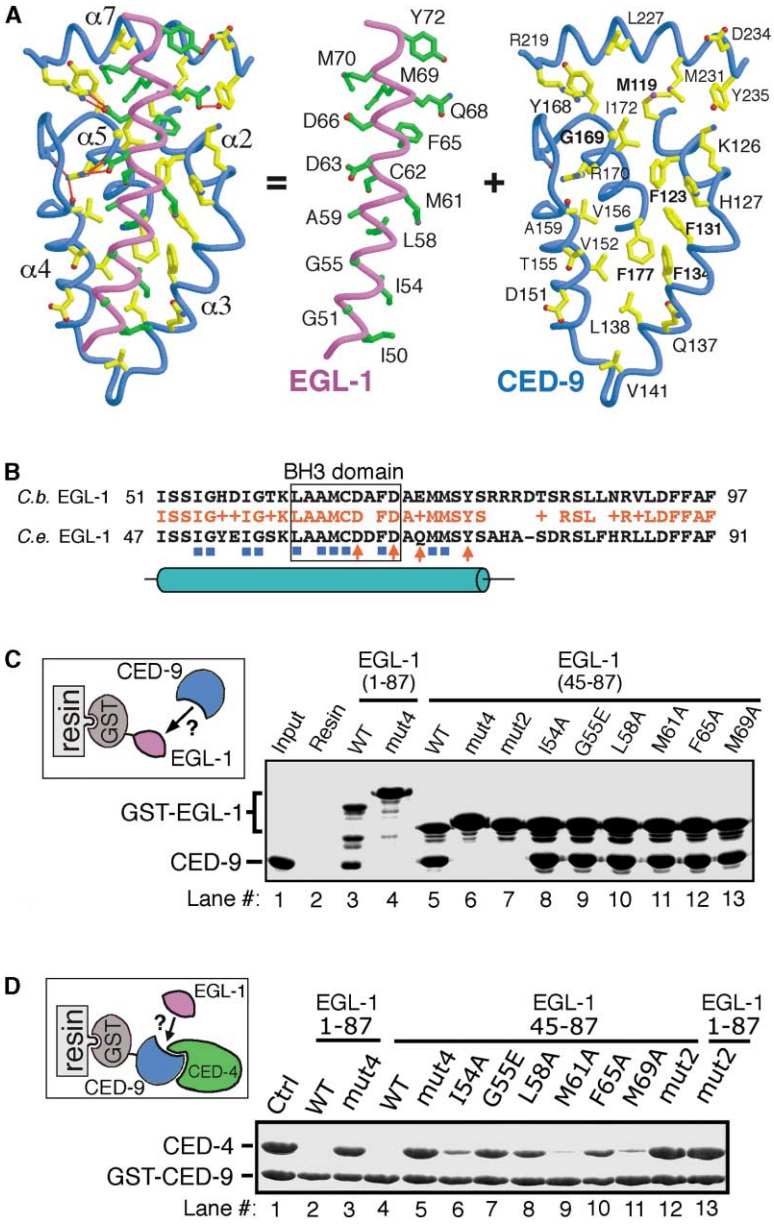

Figure 3. Biochemical and Functional Analyses of the EGL-1/CED-9 and CED-4/CED-9 Interactions

(A) A close-up view of the EGL-1/CED-9 interface. To better visualize the crowded interface, it is opened up to show its two components. The backbones of CED-9 and EGL-1 are shown in blue and pink, respectively, while their side chains are colored yellow and green, respectively. Hydrogen bonds are represented by red dashed lines.

(B) Sequence alignment of EGL-1 from two related nematode species, *C. elegans* and *C. briggsae*. The conserved residues are highlighted in red and shown between the two EGL-1 sequences. Residues involved in intermolecular van der Waals contacts and hydrogen bonds are indicated by blue square and red arrows, respectively.

(C) Biochemical analyses of the EGL-1/CED-9 interface. Mutant GST-EGL-1 fragments were immobilized on glutathione resin, and the WT CED-9 protein (Input, lane 1) was allowed to flow through the resin. After washing, what remained on the resin was visualized on SDS-PAGE followed by Coomassie staining. The two mutants, mut2 and mut4, represent G55E/F65A and G55E/L58A/F65A/M69A, respectively.

(D) The strength of EGL-1 binding to CED-9 directly correlates with the ability of EGL-1 to displace CED-4 from the CED-4/CED-9 complex.

protein and is thus relatively resistant to single missense mutations.

EGL-1 induces apoptosis by displacing CED-4 from the CED-4/CED-9 complex. To recapitulate this finding in vitro, we reconstituted a CED-4 displacement assay in which preassembled CED-4/CED-9 complex was immobilized on glutathione resin and was then challenged with various EGL-1 fragments (Figure 3D). After extensive washing, the remaining CED-4/CED-9 complex was eluted from the resin and visualized on an SDS polyacrylamide gel. As anticipated, the wild-type EGL-1 protein (residues 1–87) or the C-terminal fragment of EGL-1 (45–87) completely displaced CED-4 from the CED-4/CED-9 complex (Figure 3D, lanes 2 and 4). In contrast, most missense mutations at the EGL-1/CED-9 interface weakened the ability of EGL-1 to displace CED-4 from the CED-4/CED-9 complex. Notably, the double mutant (mut2, G55E/F65A) and quadruple mutant (mut4, G55E/L58A/F65A/M69A) completely failed to disrupt the CED-4/CED-9 complex (lanes 3, 5, 12, and 13). Interestingly, some EGL-1 mutants, such as G55E and L58A, while retaining their ability to bind to CED-9 (Figure 3C), exhibited significantly reduced ability in displacing CED-4 from the CED-4/CED-9 complex in vitro (Figure 3D, lanes 7 and 8). Hence, the ability of an EGL-1 mutant to disrupt the CED-4/CED-9 complex provides a sensitive and biologically meaningful evaluation of the effect of the EGL-1 missense mutation on its function. Our in vitro studies (Figures 3C and 3D) are in complete agreement with the structural observation (Figure 3A).

If these EGL-1 mutants were less able to disrupt the CED-4/CED-9 complex, then they should exhibit decreased ability to induce cell death compared to the WT EGL-1 protein. To examine this scenario, we injected

Table 2. Cell-Killing Activities of the Egl-1 Mutants

Transgene	Array	Average	SEM	Range
egl-1 (full length)				
	1	18.3	1.8	8–29
	2	32.4	3.9	12–67
	3	42.6	4.3	14–65
G55E and F65D				
	1	0.3	0.1	0–1
	2	0.3	0.1	0–1
	3	0.3	0.2	0–3
G55E				
	1	3.9	0.5	0–6
	2	6.4	0.5	4–12
	3	5.8	0.9	0–11
46–87				
	1	18.1	4	3–50
	2	12.6	2.3	2–30
	3	8.4	1.4	3–20
1–45				
	1	0.2	0.1	0–1
	2	0.1	0.1	0–1
	3	0.3	0.1	0–1

The *egl-1 hsp* constructs (at 25 ng/μl each) were injected into *ced-1* (*e1735*); *egl-1* (*n1084n3082*) *unc-76* (*e911*) animals with pTG96 (at 25 ng/μl), which expresses GFP in many somatic cells in most of the developmental stages, and p76-16B (at 25 ng/μl), which rescues *unc-76* uncoordinated phenotype. At least three independently transgenic lines were examined. For the heat-shock experiments, well-populated plates with many eggs were heat shocked at 33°C for 45 minutes and allowed to recover at 20°C for 3 hr. Cell corpses were scored in the anterior head region of 4-fold transgenic embryos. Fifteen animals were scored for each transgenic line. Nontransgenic embryos or transgenic embryos without heat-shock treatment have no cell corpses.

into *ced-1* (*e1735*); *egl-1* (*n1084 n3082*) animals constructs that direct expression of various EGL-1 fragments under the control of the *C. elegans* heat-shock promoters. Cell corpses were scored in the anterior head region of 4-fold transgenic embryos after the heat-shock treatment (see Experimental Procedures). Few cell corpses were observed in the *ced-1* (*e1735*); *egl-1* (*n1084 n3082*) embryos because the *egl-1* (*n1084 n3082*) mutation blocks almost all somatic cell deaths (Conradt and Horvitz, 1998). As shown previously (Conradt and Horvitz, 1998), expression of the full-length EGL-1 protein induced robust cell killing (Table 2). Interestingly, expression of the EGL-1 fragment (residues 46–87) induced about half the number of cell corpses as the full-length EGL-1, indicating that this EGL-1 fragment is functional in vivo. In contrast, expression of EGLl-1 (residues 1–45) did not induce cell death, consistent with an earlier observation (Conradt and Horvitz, 1998). In vitro, the G55E mutation in EGL-1 significantly reduced its ability to disrupt the CED-4/CED-9 complex (Figure 3D). Accordingly, EGL-1 (G55E) is a very weak cell death inducer in vivo (Table 2).

The cell-killing activity of various EGL-1 mutants correlated extremely well with their in vitro biochemical activities in binding to CED-9 and in displacing CED-4 from the CED-4/CED-9 complex. For example, in vitro, the EGL-1 double mutant (G55E/F65A) failed to bind to CED-9 (Figure 3C) or to displace CED-4 from the CED-4/CED-9 complex (Figure 3D), whereas the EGL-1 (G55E) mutant retained its ability to interact with CED-9 (Figure 3C) yet exhibited a decreased ability to disrupt the CED-4/CED-9 complex (Figure 3D). In vivo, EGL-1 (G55E/F65A) induced no cell killing while EGL-1 (G55E) induced a level of cell killing that is significantly lower than that of the wild-type EGL-1 protein (Table 2).

Biochemical Analysis of CED-4/CED-9 Interactions

To further define the molecular mechanisms by which EGL-1 induces the release of CED-4 from CED-9-mediated sequestration, we sought to identify surface residues in CED-9 that are important for binding to CED-4. We reasoned that, for molecular recognition to occur, at least some of the CED-9 residues that are important for binding to CED-4 must be solvent exposed prior to binding. Therefore, we examined the structure of CED-9 in isolation and identified a total of 44 amino acids, each with at least 30% of its surface area exposed to solvent. We grouped these 44 amino acids based on primary sequences and generated 20 CED-9 mutant clones, each containing 1–5 missense mutations but together covering all 44 solvent-exposed residues (Figures 4A and 4B). All 20 CED-9 proteins were overexpressed in *E. coli* and purified to homogeneity. Because these mutations only affect surface residues, the structural integrity of CED-9 is not affected by these mutations (data not shown).

Next, we examined the abilities of these CED-9 mutants to interact with CED-4 (Figure 4B). As anticipated, most mutations exhibited no apparent effect on the interaction between CED-9 and CED-4. In contrast, three CED-9 mutants, F146N (Figure 4B, lane 9), N158A/A159G/Q160A (lane 12), and R211E/N212G (lane 16) exhibited significantly weakened interactions with CED-4. Interestingly, although these mutations affect residues widely separated in the primary sequence, they are mapped to the same surface patch on CED-9, defining a surface motif important for CED-4 binding (Figure 4A). We believe that this surface patch constitutes the primary CED-4 binding motif, because none of the other 16 mutations affected the CED-4/CED-9 interaction, and they cover the rest of the CED-9 surface. We also confirmed a previous observation in which a missense mutation in CED-9, Y149N (*n1653ts*), was found to weaken the CED-4/CED-9 interactions (Hengartner et al., 1992) (Figure 4B, lane 10). On the CED-9 structure, however, Tyr149 is deeply buried in the hydrophobic core. Reflecting its structural role, CED-9 (Y149N) protein exhibits poor solubility, has a strong tendency to aggregate, and is prone to proteolysis (Figure 4B, lane 10).

A Working Model of How EGL-1 Disrupts CED-9/CED-4 Interactions

Our structure-based biochemical analysis revealed that CED-9 employs two distinct surface areas for its interaction with EGL-1 and CED-4. CED-9 residues that are in direct contact with EGL-1 are not involved in binding to CED-4 (Figures 3 and 4). EGL-1 binds to a hydrophobic surface cleft of CED-9; however, this hydrophobic cleft is absent in the free CED-9 protein and is only formed after major structural rearrangements induced by EGL-1 binding. These structural rearrangements primarily involve the α4 helix of CED-9 and the loop immediately following α4 (Figure 2B). Interestingly, an important part

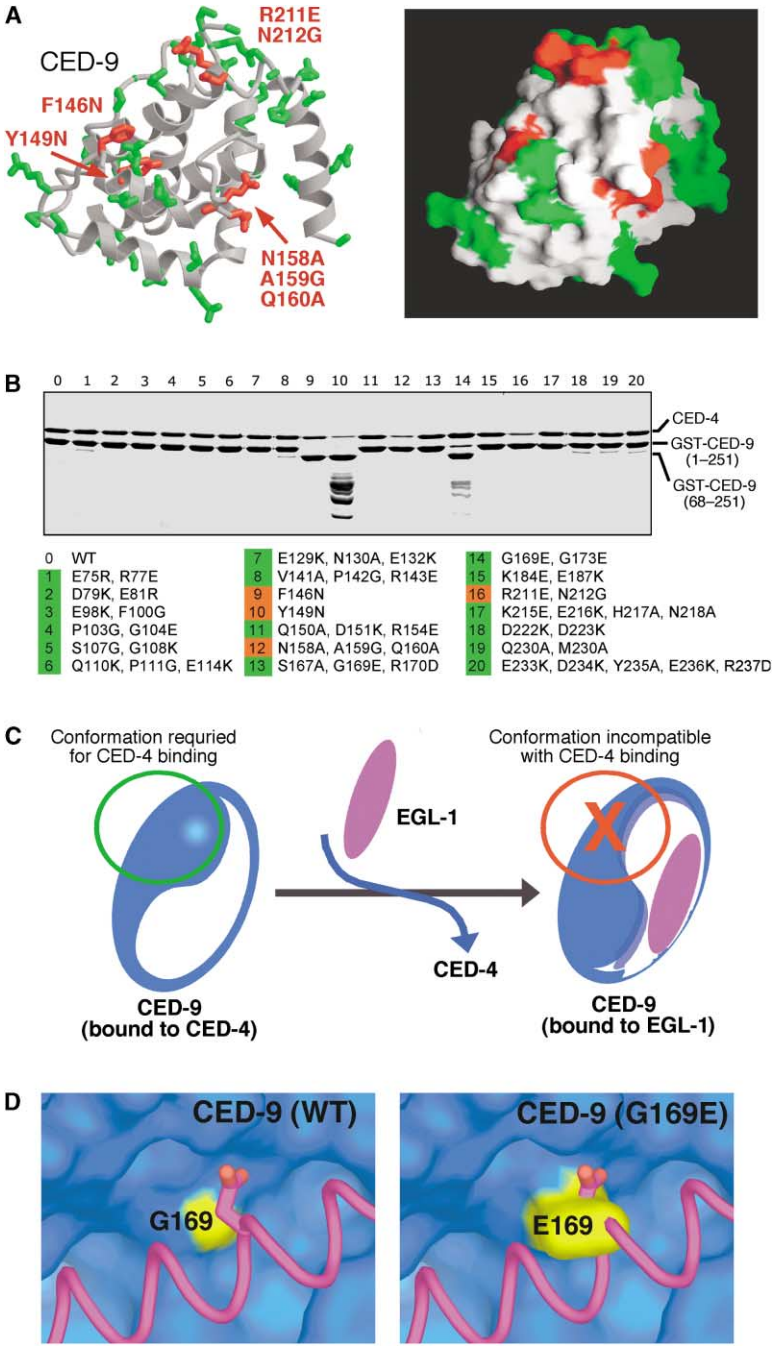

Figure 4. EGL-1 Displaces CED-4 from the CED-4/CED-9 Complex by Altering the Conformation of the CED-9 Protein

(A) Surface locations of the mutated residues in the isolated CED-9. The residues whose mutation weakened the CED-4/CED-9 interactions are highlighted in red. These mutations map to the same general area, defining a CED-4 binding surface patch. The residues whose mutation exhibited no effect on the CED-4/CED-9 interactions are shown in green.

(B) A representative SDS-PAGE analysis of CED4 binding by various CED-9 mutants. Each GST-CED-9 variant was incubated with the same amount of purified CED-4 protein. Then the protein mixture was allowed to bind to glutathione resin. After washing with buffer, the remaining CED-4/CED-9 complex was visualized on SDS-PAGE followed by Coomassie staining.

(C) A working model of how EGL-1 displaces CED-4 from the CED-4/CED-9 complex. In this model, CED-4 binds to a surface area of CED-9 that is next to the EGL-1 binding element. The CED-9 conformational change induced by EGL-1 binding results in the disruption of the CED-4/CED-9 complex.

(D) Mechanism of the gain-of-function mutation G169E in CED-9. Gly169 maps to the EGL-1 binding pocket (left panel). As previously predicted (Parrish et al., 2000), the replacement of Gly169 by Glu creates severe steric clash with the backbone of EGL-1 (right panel).

of the CED-4 binding element in CED-9, involving residues 158–160 (Figure 4B), maps to this loop. This observation indicates that the binding of EGL-1 to CED-9 will inevitably induce a drastic rearrangement of the loop following helix α4 and thus destabilize the binding of CED-4 to CED-9, leading to the release of CED-4 from the CED-4/CED-9 complex.

These data and analyses strongly suggest a working model by which EGL-1 displaces CED-4 from the CED-4/CED-9 complex (Figure 4C). In this model, CED-4 binds to a surface area of CED-9 that is next to the EGL-1 binding element. This interaction allows CED-9 to sequester CED-4 to the outer membrane of mitochondria (Chen et al., 2000). At the onset of programmed cell death, the EGL-1 protein is expressed and binds to CED-9. The drastic conformational changes in the α4 loop region of CED-9 induced by EGL-1 binding results in the disruption of the CED-4/CED-9 complex, because the specific conformation of EGL-1-bound CED-9 is not compatible with that required for binding to CED-4 (Figure 4C).

This model is supported by our structural and biochemical analyses and explains a body of published observations. For example, G169E in CED-9 was a gain-of-function mutation (Hengartner and Horvitz, 1994a). This mutation affects a small residue that is in the EGL-1

binding pocket (Figure 4D, left panel) and away from the CED-4 binding surface patch. Hence, the replacement of Gly169 by the bulky Glu is expected to generate steric clash with EGL-1 (Figure 4D, right panel), thus negatively affecting EGL-1 binding but having no impact on CED-4 binding (Parrish et al., 2000). Indeed this has been proven to be the case (Parrish et al., 2000). We also experimentally confirmed this prediction (data not shown).

In conclusion, our combined structural, biochemical, and functional studies have identified the molecular mechanisms by which EGL-1 binds to CED-9 and induces the release of CED-4 from the CED-4/CED-9 complex. These studies define a mechanistic framework for understanding apoptosis activation in *C. elegans*.

Experimental Procedures

Protein and Peptide Preparation

All constructs were generated using a standard PCR-based cloning strategy. For EGL-1/CED-9 interaction assays, EGL-1 and CED-9 were coexpressed in vectors pGEX-2T (Pharmacia) and pBB75, respectively. For CED-4/CED-9 disruption assays, all EGL-1 proteins were overexpressed in *E. coli* strain BL21 (DE3) as GST fusion proteins using pGEX-2T. To obtain a CED-4/CED-9 complex, CED-9 and CED-4 were coexpressed in vectors pGEX-2T and pBB75, respectively. Proteins were purified to homogeneity as described (Chai et al., 2001).

Crystallization and Data Collection

Crystals of CED-9 (residues 68–237) in complex with EGL-1 (residues 31–87 or 45–87) were obtained by the hanging-drop vapor-diffusion method by mixing the complex with reservoir solution containing 50 mM NaCacodylate (pH 6.5), 100 mM ammonium acetate, 15 mM magnesium acetate, 12% tert-butanol, and 5 mM dithiothreitol (DTT). The crystals belong to the space group $P4_3$ and contain two complexes in each asymmetric unit. The unit cell dimensions are $a = b = 193.7$ Å, and $c = 57.45$ Å. Crystals were equilibrated in a cryoprotectant buffer containing well buffer plus 20% glycerol and were flash frozen in a −170°C nitrogen stream. The native data were collected at the CHESS beamline A1. Data were processed using the software Denzo and Scalepack (Otwinowski and Minor, 1997).

Structure Determination

The structure was determined by molecular replacement, using AMoRe (Navaza, 1994). The atomic model was built using O (Jones et al., 1991) and refined using CNS (Terwilliger and Berendzen, 1996). The electron density for the bound EGL-1 fragment became unambiguous after preliminary refinement. The final refined atomic model contains residues 74–237 of CED-9 and residues 47–73 of EGL-1 at 2.2 Å resolution. The N-terminal 2 residues and the C-terminal 14 residues in EGL-1 have no electron density in the maps, and we presume that these regions are disordered in the crystals.

GST-Mediated Pull-Down Assay

0.4 mg recombinant EGL-1 variant was bound to 200 μl of glutathione resin. The resin was washed with 400 μl buffer for four times to remove excess unbound protein. Then 600 μg of the CED-9 protein was allowed to flow through the resin. After washing with buffer A containing 25 mM Tris (pH 8.0), 150 mM NaCl, and 2 mM DTT, GST-EGL-1 was eluted with 5 mM reduced glutathione, and all fractions were visualized by SDS-PAGE with Coomassie staining.

CED-4/CED-9 Disruption Assay

Approximately 0.4 mg of purified 1:1 complex of GST-CED-9/CED-4 was immobilized on glutathione sepharose 4B resin. Excess EGL-1 fragment was incubated with the resin for 10 min and was allowed to flow through. After washing with buffer A, GST-CED-9/CED-4 was eluted and visualized on SDS-PAGE.

Cell-Killing Assays

ced-1 (*e1735*); *egl-1* (*n1084 n3082*) *unc-76* (*e911*) animals were injected with Psur-5GFP, unc-76, and the indicated EGL-1 fragment under the control of the heat-shock promoters each at 25 ng/μl. Each transgenic line was independently generated. Well-populated plates with many eggs were heat shocked at 33°C for 45 min and allowed to recover at 20°C for 3 hr. Cell corpses were scored in the anterior head region of 4-fold embryos. Fifteen animals were scored for each experiment.

CED-9 Mutants and CED-4 Binding Assay

All 20 CED-9 variants were overexpressed as GST fusion proteins, purified as described (Chai et al., 2001), and quantified by UV spectroscopy. The same amount of each CED-9 variant was incubated with purified CED-4 protein at a molar ratio of 1:1. The final concentration of each protein was approximately 3 μM. 500 μl of each protein mixture was incubated with 100 μl glutathione resin for 20 min. After washing with buffer A, the remaining CED-4/CED-9 complex was eluted and visualized on SDS-PAGE.

Acknowledgments

We thank Bob Horvitz for numerous reagents, Lana Walsh for beam time at CHESS, Amy Cocina, Ewina Fung, and Min Hu for technical assistance, and T.K. Vanderlick and M. Apel-Paz for help with ITC. This research was supported by NIH grants.

Received: May 13, 2004
Revised: June 28, 2004
Accepted: July 9, 2004
Published: September 23, 2004

References

Chai, J., Wu, Q., Shiozaki, E., Srinivasula, S.M., Alnemri, E.S., and Shi, Y. (2001). Crystal structure of a procaspase-7 zymogen: mechanisms of activation and substrate binding. Cell *107*, 399–407.

Chen, F., Hersh, B.M., Conradt, B., Zhou, Z., Riemer, D., Gruenbaum, Y., and Horvitz, H.R. (2000). Translocation of C. elegans CED-4 to nuclear membranes during programmed cell death. Science *287*, 1485–1489.

Chinnaiyan, A.M., O'Rourke, K., Lane, B.R., and Dixit, V.M. (1997). Interaction of CED-4 with CED-3 and CED-9: a molecular framework for cell death. Science *275*, 1122–1126.

Conradt, B., and Horvitz, H.R. (1998). The C. elegans protein EGL-1 is required for programmed cell death and interacts with the Bcl-2-like protein CED-9. Cell *93*, 519–529.

Cory, S., Huang, D.C., and Adams, J.M. (2003). The Bcl-2 family: roles in cell survival and oncogenesis. Oncogene *22*, 8590–8607.

del Peso, L., Gonzalez, V.M., and Nunez, G. (1998). Caenorhabditis elegans EGL-1 disrupts the interaction of CED-9 with CED-4 and promotes CED-3 activation. J. Biol. Chem. *273*, 33495–33500.

del Peso, L., Gonzalez, V.M., Inohara, N., Ellis, R.E., and Nunez, G. (2000). Disruption of the CED-9.CED-4 complex by EGL-1 is a critical step for programmed cell death in Caenorhabditis elegans. J. Biol. Chem. *275*, 27205–27211.

Hengartner, M.O., and Horvitz, H.R. (1994a). Activation of C. elegans cell death protein CED-9 by an amino-acid substitution in a domain conserved in Bcl-2. Nature *369*, 318–320.

Hengartner, M.O., and Horvitz, H.R. (1994b). C. elegans cell survival gene ced-9 encodes a functional homolog of the mammalian proto-oncogene bcl-2. Cell *76*, 665–676.

Hengartner, M.O., Ellis, R.E., and Horvitz, H.R. (1992). Caenorhabditis elegans gene ced-9 protects cells from programmed cell death. Nature *356*, 494–499.

Horvitz, H.R. (1999). Genetic control of programmed cell death in the nematode Caenorhabditis elegans. Cancer Res. *59*, 1701–1706.

Horvitz, H.R. (2003). Worms, Life, and Death (Nobel Lecture). Chembiochem *4*, 697–711.

Irmler, M., Hofmann, K., Vaux, D., and Tschopp, J. (1997). Direct

physical interaction between the Caenorhabditis elegans 'death proteins' CED-3 and CED-4. FEBS Lett. *406*, 189–190.

James, C., Gschmeissner, S., Fraser, A., and Evan, G.I. (1997). CED-4 induces chromatin condensation in Schizosaccharomyces pombe and is inhibited by direct physical association with CED-9. Curr. Biol. *7*, 246–252.

Jones, T.A., Zou, J.-Y., Cowan, S.W., and Kjeldgaard, M. (1991). Improved methods for building protein models in electron density maps and the location of errors in these models. Acta Crystallogr. *A47*, 110–119.

Liu, X., Dai, S., Zhu, Y., Marrack, P., and Kappler, J.W. (2003). The structure of a Bcl-xL/Bim fragment complex: implications for Bim function. Immunity *19*, 341–352.

Navaza, J. (1994). AMoRe: an automated package for molecular replacement. Acta Crystallogr. *A50*, 157–163.

Otwinowski, Z., and Minor, W. (1997). Processing of X-ray diffraction data collected in oscillation mode. Methods Enzymol. *276*, 307–326.

Parrish, J., Metters, H., Chen, L., and Xue, D. (2000). Demonstration of the in vivo interaction of key cell death regulators by structure-based design of second-site suppressors. Proc. Natl. Acad. Sci. USA *97*, 11916–11921.

Petros, A.M., Nettesheim, D.G., Wang, Y., Olejniczak, E.T., Meadows, R.P., Mack, J., Swift, K., Matayoshi, E.D., Zhang, H., Thompson, C.B., and Fesik, S.W. (2000). Rationale for Bcl-xL/Bad peptide complex formation from structure, mutagenesis, and biophysical studies. Protein Sci. *9*, 2528–2534.

Puthalakath, H., and Strasser, A. (2002). Keeping killers on a tight leash: transcriptional and post-translational control of the pro-apoptotic activity of BH3-only proteins. Cell Death Differ. *9*, 505–512.

Sattler, M., Yoon, H.S., Nettesheim, D., Meadows, R.P., Harlan, J.E., Eberstadt, M., Yoon, H.S., Shuker, S.B., Chang, B.S., Minn, A.J., et al. (1997). Structure of Bcl-xL-Bak peptide complex: recognition between regulators of apoptosis. Science *275*, 983–986.

Seshagiri, S., and Miller, L.K. (1997). Caenorhabditis elegans CED-4 stimulates CED-3 processing and CED-3-induced apoptosis. Curr. Biol. *7*, 455–460.

Shi, Y. (2002). Mechanisms of caspase inhibition and activation during apoptosis. Mol. Cell *9*, 459–470.

Spector, M.S., Desnoyers, S., Hoeppner, D.J., and Hengartner, M.O. (1997). Interaction between the C. elegans cell-death regulators CED-9 and CED-4. Nature *385*, 653–656.

Terwilliger, T.C., and Berendzen, J. (1996). Correlated phasing of multiple isomorphous replacement data. Acta Crystallogr D Biol. Crystallogr. *52*, 749–757.

Woo, J.S., Jung, J.S., Ha, N.C., Shin, J., Kim, K.H., Lee, W., and Oh, B.H. (2003). Unique structural features of a BCL-2 family protein CED-9 and biophysical characterization of CED-9/EGL-1 interactions. Cell Death Differ. *10*, 1310–1325.

Wu, D., Wallen, H.D., Inohara, N., and Nunez, G. (1997a). Interaction and regulation of the Caenorhabditis elegans death protease CED-3 by CED-4 and CED-9. J. Biol. Chem. *272*, 21449–21454.

Wu, D., Wallen, H.D., and Nunez, G. (1997b). Interaction and regulation of subcellular localization of CED-4 by CED-9. Science *275*, 1126–1129.

Xue, D., Shaham, S., and Horvitz, H.R. (1996). The Caenorhabditis elegans cell-death protein CED-3 is a cysteine protease with substrate specificities similar to those of the human CPP32 protease. Genes Dev. *10*, 1073–1083.

Yang, X., Chang, H.Y., and Baltimore, D. (1998). Essential Role of CED-4 Oligomerization in CED-3 Activation and Apoptosis. Science *281*, 1355–1357.

Yuan, J., and Horvitz, H.R. (1992). The Caenorhabditis elegans cell death gene ced-4 encodes a novel protein and is expressed during the period of extensive programmed cell death. Development *116*, 309–320.

Yuan, J., Shaham, S., Ledoux, S., Ellis, H.M., and Horvitz, H.R. (1993). The C. elegans cell death gene Ced-3 encodes a protein similar to mammalian interleukin-1 beta-converting enzyme. Cell *75*, 641–652.

Accession Numbers

The atomic coordinates of the EGL-1/CED-9 complex have been deposited in the Protein Data Bank under the accession number 1TY4.